13th World Conference on Earthquake Engineering
Vancouver, B.C., Canada
August 1-6, 2004
Paper No. 1699

AXIAL COLLAPSE OF REINFORCED CONCRETE COLUMNS

Manabu YOSHIMURA [1], Yoshikazu TAKAINE[2] and Takaya NAKAMURA[3]

SUMMARY

Half-scale specimens with shear or flexure-shear failure modes simulating RC columns designed by the old code in Japan were tested until they came to be unable to sustain axial load. Test variables were longitudinal reinforcement, axial load and transverse reinforcement. Using the results from this test and the past similar tests, the general nature of column collapse including lateral drift associated with the collapse was discussed. Some structural indices that were considered to govern the collapse drift were also studied.

INTRODUCTION

The minimum performance that columns are required during severe earthquakes is to support axial load. During past severe earthquakes, a number of RC columns designed by the old code failed in shear (Photo 1(a)) and eventually came to be unable to sustain axial load or collapsed. To evaluate ultimate seismic performance of old columns, it is necessary to grasp how they reached the collapse and how much the drift associated with the collapse was. However, researches on this issue are very scarce.

Moehle et al. proposed the equation that predicted the collapse drift, Moehle [1]. Whereas this equation did not take account of the effect of longitudinal reinforcement on the collapse drift, some tests have revealed it heightens the collapse drift, Nakamura [2]. This is an interesting issue to be discussed.

At past earthquakes, amongst rather long columns, some failed in shear after flexural yielding (Photo. 1(b)) while most of the others failed in shear without experiencing flexural yielding. This paper is intended to study the collapse of rather long columns with $h_0/D=4$ (h_0: column clear height, D: column depth) that may result in either failure mode. And using the results of this test and the past tests done for $h_0/D=3$ and 2, Nakamura [3 and 2, respectively], the combined effect of longitudinal reinforcement and axial load on the collapse drift, and the application of the above equation to these tests are studied. The relations between the ratio of computed shear strength to computed flexural strength that is often used to assess column deformability and the collapse drift are also investigated.

[1] *Professor, Department of Architecture, Tokyo Metropolitan University, Japan. E-mail:myoshim@arch.metro-u.ac.jp*
[2] *Graduate Student, Department of Architecture, Tokyo Metropolitan University, Japan. E-mail takaine@ecomp.metro-u.ac.jp*
[3] *Research Assoc., Department of Architecture, Tokyo Metropolitan University, Japan. E-mail:takaya@ecomp.metro-u.ac.jp*

(a) Shear failure (b) Flexure-Shear failure

Photo 1: Real damage (1995 Kobe Earthquake)

OUTLINE OF TEST

Eight half-scale specimens simulating columns designed by the old code are summarized in Table 1 and an example of reinforcement details is shown in Figure 1. They were designed so that shear failure or shear failure after flexural yielding might result. A column section (b×D=300mm×300mm), column clear height (h_0=1200mm) were uniform. Test variables were: 1) longitudinal bar ratio, p_g=2.65%, 1.69% and 0.94%, 2) axial stress ratio, η= 0.20, 0.30 and 0.35, and 3) transverse bar ratio, p_w=0.21%, 0.14% and 0.11%. Material properties are listed in Tables 2 and 3.

Test apparatus is shown in Figure 2, where the pantograph was placed so that the loading beam at the column top did not rotate (double curvature deformation was realized). A loading method was as follows. The specimens were loaded to the lateral direction under constant vertical load. The vertical actuator was controlled by load while the lateral actuator was by displacement. And the test was terminated by the limiter of the vertical actuator that was set to operate when vertical deformation (axial shortening) reached 50mm.

The general rule of loading was such that the specimens were displaced to the positive direction until collapse after subjected to a full reversal with drift angle of 0.5%, 1% and 2%. However, some specimens collapsed during the reversed loading.

Table 1: Structural properties of specimens

<table>
<tr><th>Name</th><th>h_0
(mm)</th><th>b×D
(mm)</th><th>h_0/D</th><th>p_g (%)</th><th>η (1)</th><th>p_w (%)</th></tr>
<tr><td>No.1</td><td rowspan="8">1200</td><td rowspan="8">300×300</td><td rowspan="8">4</td><td rowspan="5">2.65
(12-D16)</td><td rowspan="3">0.20</td><td>0.21(2-D6@100)</td></tr>
<tr><td>No.2</td><td>0.14(2-D6@150)</td></tr>
<tr><td>No.3</td><td>0.11(2-D6@200)</td></tr>
<tr><td>No.4</td><td>0.30</td><td>0.21(2-D6@100)</td></tr>
<tr><td>No.5</td><td>0.35</td><td>0.21(2-D6@100)</td></tr>
<tr><td>No.6</td><td rowspan="2">1.69
(12-D13)</td><td rowspan="3">0.20</td><td>0.21(2-D6@100)</td></tr>
<tr><td>No.7</td><td>0.14(2-D6@150)</td></tr>
<tr><td>No.8</td><td>0.94
(12-D10)</td><td>0.14(2-D6@150)</td></tr>
</table>

(1) $\eta=N/(bD\sigma_B)$ (N: Axial load, σ_B: Concrete strength)

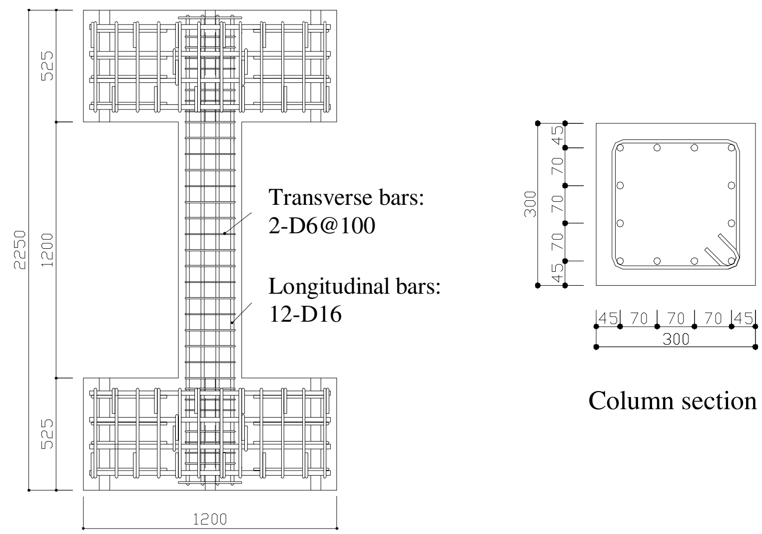

Figure 1: Reinforcement details of specimen (No. 1)

Table 2: Material properties of steel

	Yield stress (N/mm^2)	Yield strain (%)
D16	402	0.240
D13	409	0.232
D10	388	0.220
D6	392	0.235

Table 3: Material properties of concrete

Max. stress (N/mm^2)	Strain at max. stress (%)
30.7	0.222

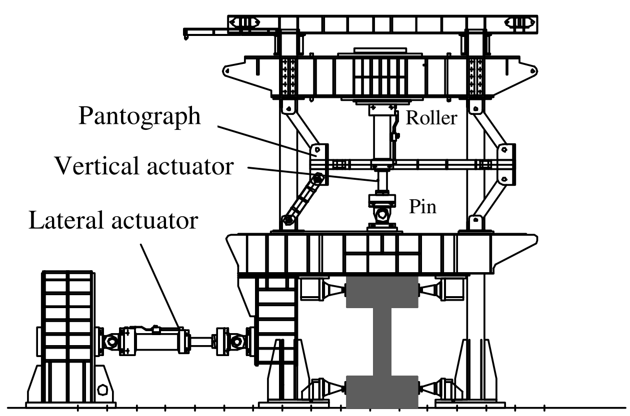

Figure 2: Test apparatus

TEST RESULTS

General

No.1 through No.5 failed in shear without flexural yielding, while No.6 through No.7 failed in shear after flexural yielding and No.8 failed in flexure after flexural yielding. All specimens finally collapsed. Maximum drift that the specimens had experienced by the moment of the collapse was denoted as collapse drift. When drift was large, shear force (force acting on the direction perpendicular to the column axis) a little differed from the lateral load applied by the lateral actuator. Shear force V was determined by the following equation.

$$V = H\, cos\, R + N\, sin\, R \tag{1}$$

where H: lateral load, R: drift angle, and N: axial load.

Observed results and computed strength are summarized in Table 4 (IS drift angle is explained later). Damage conditions and drift angle vs. shear relations for selected specimens are shown in Photo 2 and Figure 3.

Table 4: Observed results and computed strength

Name	Max. shear (kN)	Shear failure		Collapse		Computed strength			Failure mode (1)
		Drift angle (%)	IS drift angle (%)	Drift angle (%)	IS drift angle (%)	Flexure (kN)	Shear (kN)	Strength ratio	
No.1	234	0.57	0.38	13.4	8.9	241	177	0.73	S
No.2	230	0.58	0.39	5.4	3.6	241	167	0.69	S
No.3	230	0.38	0.25	2.0	1.3	241	162	0.67	S
No.4	261	0.73	0.49	2.0	1.3	276	197	0.71	S
No.5	275	1.3	0.87	2.0	1.3	288	208	0.72	S
No.6	219	5.3	3.6	5.3	3.6	195	168	0.86	FS
No.7	213	2.0	1.3	2.0	1.3	195	159	0.82	FS
No.8	174	17.9	11.9	17.9	11.9	156	150	0.96	F

(1) S: Shear, FS: Flexure-Shear and F: Flexure

Specimens with Shear Mode

No.1, No.3 and No.4 failed in shear at point A in Figure 3(a), when a shear crack occurred at the column middle portion. At that moment the transverse bars that the shear crack crossed yielded and shear force dropped (point A$\rightarrow$point B). However, the collapse did not occur at that time. The shear crack widened during the subsequent loading, and when shear force decreased nearly to zero, the collapse occurred. The buckling of longitudinal bars and the fracture or loosing at the hook of transverse bars were observed at the column middle portion. All specimens with the shear mode exhibited similar procedures to the collapse.

The procedures to the collapse are discussed for No.3 using measured strains of the longitudinal bars. Figure 4 shows the locations where strains of longitudinal bars were measured. Strain gauges were attached at two sides of the bars. The strains measured at locations, L1, L2 and L3 are shown in Figure 5 for the loading aiming at drift angle of –1% where shear failure occurred. The value of strains is an average of those at the two sides. After point A, the strain at L2 that was near the shear crack began to deviate from those at L1 and L3. The two stains at L2 are shown in Figure 6. They went to the opposite direction after point A throughout the loading aiming at drift angle of –1%. This was because local (flexural) deformation occurred on this bar at L2 due to the shear crack. The widening of the shear crack lead to the increase of the local deformation, resulting in the decrease of compression carrying capacity of this bar. On the other hand, after the point of drift angle of –1%, average strains at L2 were observed to proceed to compression, indicating that the compression carried by this bar increased probably because the contact area of concrete above and below the shear crack decreased as the shear crack widened. The above behavior is schematically depicted in Figure 7. The locations of longitudinal bars where the local deformation was confirmed, are shown in Figure 8. The occurrence of the local deformation was judged whether the strains at the two sides proceeded to the opposite direction. It is apparent the local deformation of the longitudinal bars occurred at the locations along the shear crack.

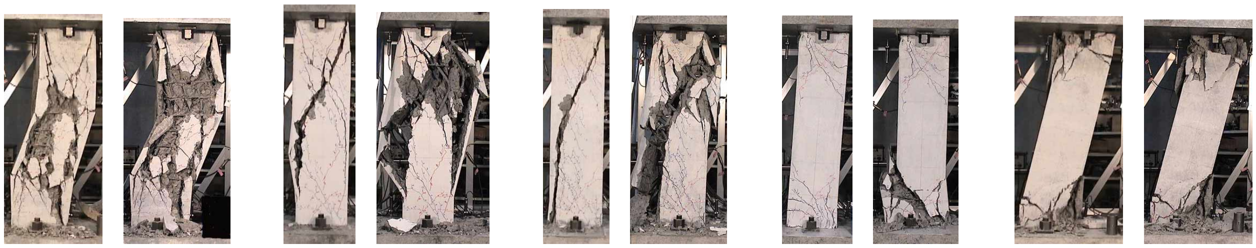

At collapse After collapse | At collapse After collapse | At collapse After collapse | At +5% After collapse | At collapse After collapse

(a) No.1 **(b) No.3** **(c) No.4** **(d) No.6** **(e) No.8**

Photo 2: Damage condition

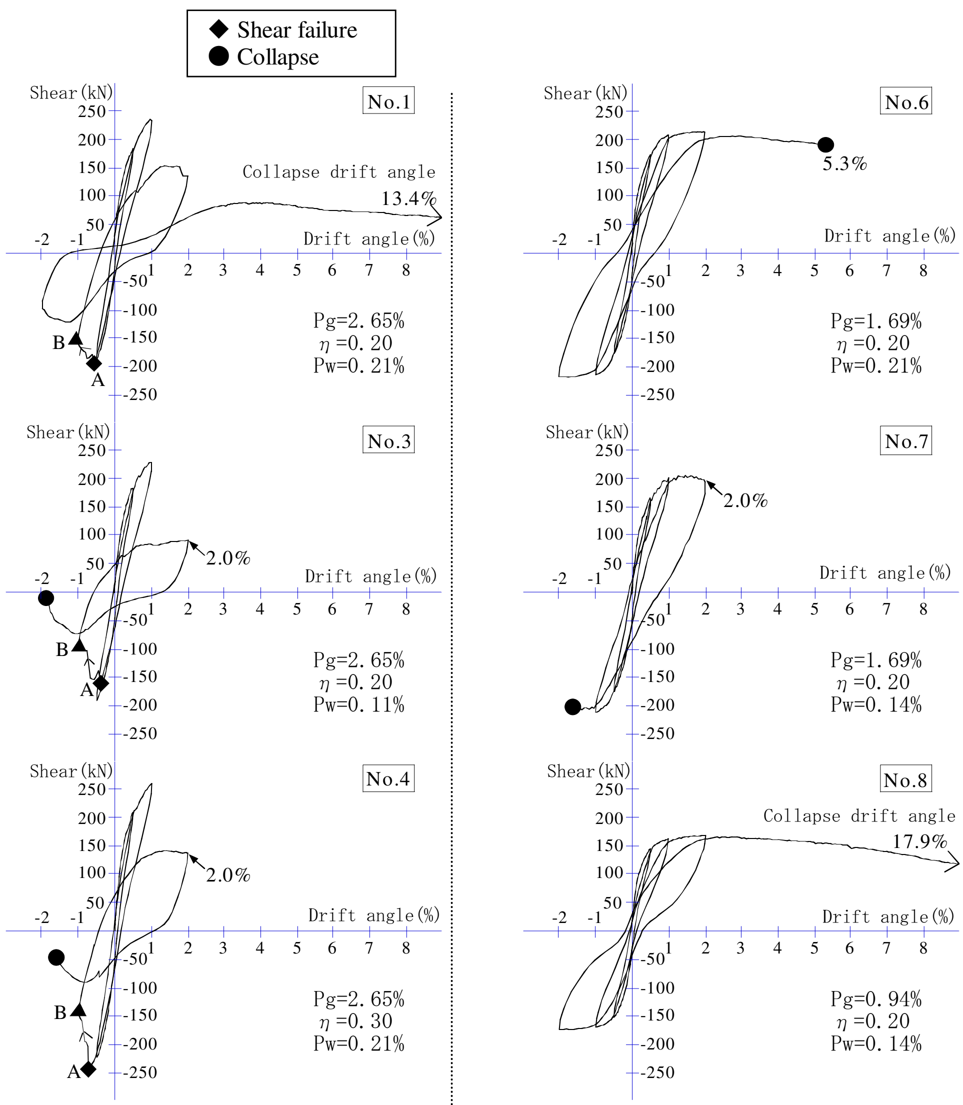

(a) Shear mode **(b) Flexure-Shear mode (No.8: Flexure mode)**

Figure 3: Drift angle vs. shear force

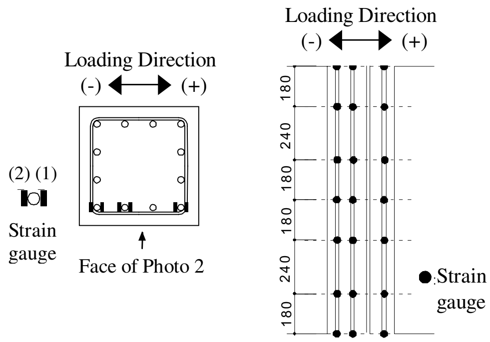

Figure 4: Strain measurement (Longi. bars)

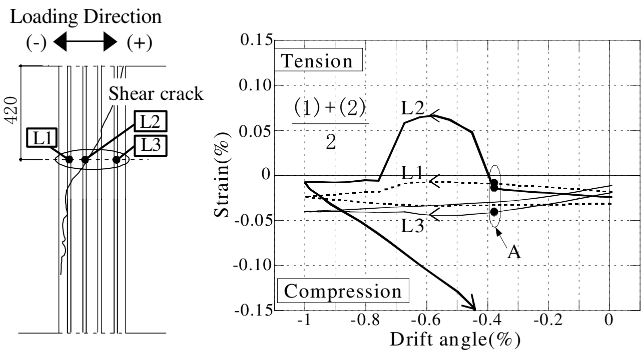

Figure 5: Drift angle vs. strain (Longi. bars, No.3)

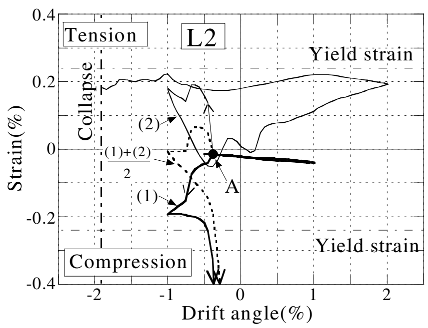

Figure 6: Drift angle vs. strain (Longi. bar, No.3)

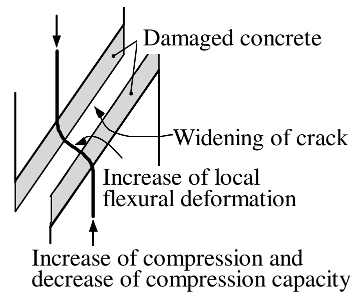

Figure 7: Behavior of longi. bar near shear crack

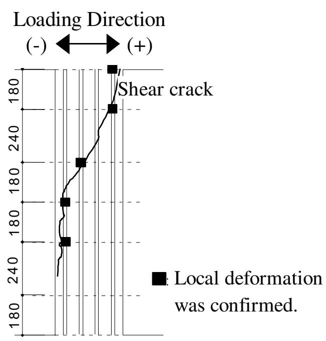

Figure 8: Location of longi. bars with local deformation (No. 3)

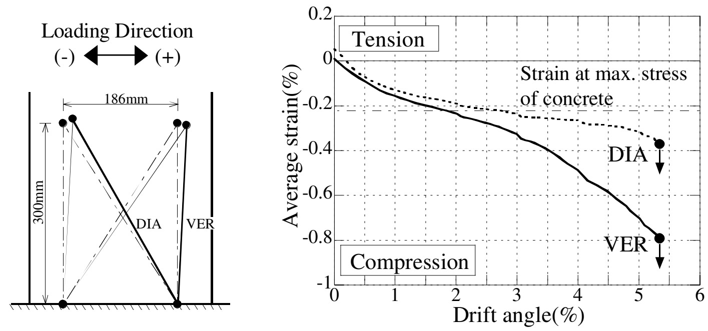

Figure 9: Drift angle vs. average strain (No.6)

Specimens with Flexure-Shear or Flexure Mode

No.6 and No.7 that first yielded in flexure failed in shear at the hinge region due to the sudden crushing of concrete (compression-shear failure), and the collapse occurred simultaneously. The collapse occurred without any symptom of it. The buckling of longitudinal bars, and the fracture or loosing at the hook of transverse bars were observed at the hinge region. No.8 that yielded in flexure failed in flexure at the hinge region, and the collapse occurred simultaneously. The procedures to the collapse of this specimen were similar to those of No.6 and No.7.

Average strains at the hinge region were measured by displacement transducers. Drift angle vs. average strain relations are shown in Figure 9 for No.6 at two locations, VER and DIA. Compression strains at VER increased with the increase of drift angle, reaching as much as 0.8% at the collapse, indicating that the damage to concrete had become severe before the collapse. Compression strains at DIA were also large, 0.4% at the collapse, indicating the concrete was subjected to large compression strains due to shear force as well as bending moment. Thus, those specimens with the flexure-shear mode collapsed because of the crushing of concrete at the hinge region.

Effect of Test Variables on Collapse Drift

The specimens with the shear mode and flexure-shear mode (hereafter, the latter includes flexure mode for the sake of convenience) differed in the collapse mechanism. The effect of test variables on the collapse drift was studied for each mode. The combinations of test variables are shown in Figure 10. For the specimens with the shear mode, if p_g and axial load were same, the collapse drift angle increased with the increase of p_w: No.1 (13.4%)>No.2 (5.4%)>No.3 (2.0%). And if p_g and p_w were same, it in general increased with the decrease of axial load: No.1 (13.4%)>No. 4 (2.0%)=No.5 (2.0%). For the specimens with the flexure-shear mode, if p_g and axial load were same, the collapse drift angle was larger for larger p_w: No.6 (5.3%)>No.7 (2.0%). And if axial load and p_w were same, it was larger for smaller p_g: No.8 (17.9%)>No.7 (2.0%).

On the other hand, the comparison of the specimens that had a different failure mode because of different p_g and same axial load and p_w, revealed that the collapse drift angle was larger for the shear mode than for the flexure-shear mode: No.1 (13.4%)>No.6 (5.3%) and No.2 (5.4%)>No.7 (2.0%). It is interesting to note these results are opposite to the general recognition that specimens with the shear mode are inferior in deformability to those with the flexure-shear mode. This is discussed later again.

COLLAPSE DRIFT OF SPECIMENS WITH SHEAR MODE

Combined Effect of Longitudinal Reinforcement and Axial Load on Collapse Drift

For the specimens with the shear mode, as drift increased or a shear crack widened, longitudinal bars near the shear crack attracted more axial compression while the compression strength of them decreased. It suggests that the longitudinal bars have a significant role on the collapse. Hence, a ratio of axial load to initial compression strength of the longitudinal bars, η_s (bar stress ratio) was introduced.

$$\eta_s = N /(A_s \cdot \sigma_y) \qquad (2)$$

where N: axial load, A_s: total area of longitudinal bars, and σ_y: yield stress of them.

Five specimens with the shear mode tested this time and other ten with the same mode tested earlier were studied. The totally fifteen specimens were different in the column clear height (h_0=600mm, 900mm and 1200mm). Therefore, same drift angle does not mean same drift. In addition, from the practical viewpoint it would be convenient if drift angle is expressed in terms of interstory (IS) drift angle of full-scale buildings. Collapse drift angle was translated to collapse IS drift angle, and η_s vs. collapse IS drift angle relations were discussed.

The way to translate drift angle into IS drift angle was as follows. A full-scale building with particular geometric properties, as shown in Figure 11, was assumed. The specimens were deemed to be half-scale models of the columns in this building. Let H_0 be story height. Then collapse IS drift angle R_{st} is obtained from drift angle R.

$$R_{ST} = \left(h_0 / H_0\right)\cdot R \qquad (3)$$

Major results of the past tests including R_{st} are tabulated in Table 5.

The relation between η_s and collapse IS drift angle are shown in Figure 12. The range of test variables were as follows: h_0/D=2 to 4, p_g=1.69%, 2.65%, η =0.18 to 0.35 and p_w=0.11% to 0.21%. No.2 and No.3 alone were 0.11% and 0.14% in p_w. For the remaining thirteen specimens with p_w of 0.21%, the collapse IS drift angle tended to increase as η_s decreased, although plots were widely scattered. This suggests that if p_w is same, the collapse IS drift angle may be evaluated using the bar stress ratio η_s that includes the effect of p_g and axial load. As stated earlier, the results of No.1, No.2 and No.3 that were different in p_w and same in η_s (0.58) showed that as p_w increased, the collapse ID drift angle increased. In consideration that the result of No.3 that is minimum in p_w (0.11%) is 1.3%, it can be said if p_w is more than 0.1% and η_s is less than 0.6, the collapse IS drift angle of 1% is secured.

The results of 2C and 2C13 that are identical except for p_g indicates that as p_g is more or η_s is less, the collapse IS drift angle is larger.

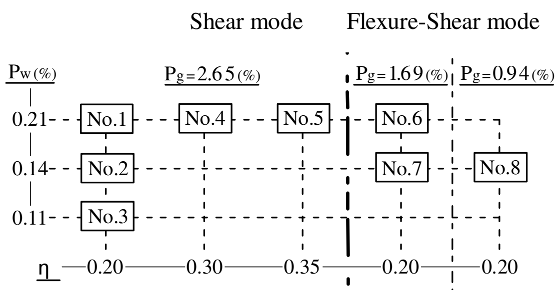

Figure 10: Combinations of test variables

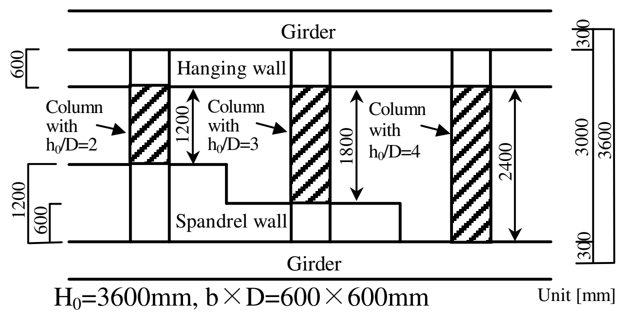

Figure 11: Assumed full-scale building

Table 5: Results of past tests

Name	h_0 (mm)	b×D (mm)	h_0/D	p_g (%)	η	p_w (%)	Strength ratio	Shear failure		Collapse	
								Drift angle (%)	IS drift angle (%)	Drift angle (%)	IS drift angle (%)
N18M	900	300 × 300	3	2.65	0.18	0.21	0.65	0.80	0.40	10.3	5.2
N18C								0.93	0.46	20.6	10.3
N27M					0.27		0.62	0.78	0.39	4.7	2.4
N27C								0.54	0.27	3.0	1.5
2M	600	300 × 300	2	2.65	0.19	0.21	0.52	0.66	0.22	11.2	3.7
2C								0.27	0.09	7.8	2.6
3M					0.29		0.49	0.60	0.20	5.6	1.9
3C								0.72	0.24	5.3	1.8
2M13				1.69	0.19		0.66	0.43	0.14	4.1	1.4
2C13								0.47	0.15	3.0	1.0

Existing Equation That Predicts Collapse Drift Angle

Moehle et al. proposed the equation to predict the collapse drift angle using shear-friction model. This equation was applied to the above fifteen specimens. A free body of a column upper portion subjected to shear force and axial load is shown in Figure 13, where V=0, V_d=0 and P_s=0 are assumed. Note that the compression carried by longitudinal bars were assumed zero. Observed and computed collapse drift angles are compared in Figure 14. The agreement was good in case of large values of η_s (η_s>0.6).

However, in case of small values of η_s ($\eta_s \leq 0.6$) the computed values were considerably smaller than the observed ones. Let us compare the results of 2C and 2C13. For 2C that had a small value of η_s, the computed result underestimated the observed one, while for 2C13 the agreement was fairly good. It may be due to that this model ignores the effect of longitudinal bars on the compression carrying capacity. The collapse drift angles computed for 2C by assuming P_s=0 and P_s=0.2 $A_s\sigma_y$ are compared in Figure 15. By considering the effect of longitudinal bars on the compression carrying capacity, the computed value became larger. The equation may be improved if this effect is appropriately included.

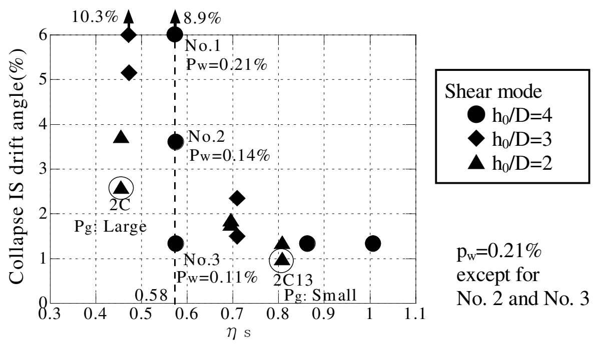

Figure 12: η_s vs. collapse IS drift angle

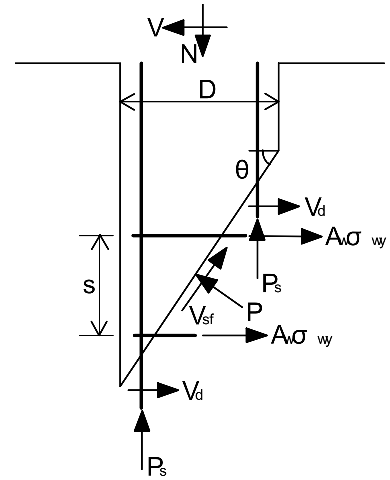

Figure 13: Free body after shear failure

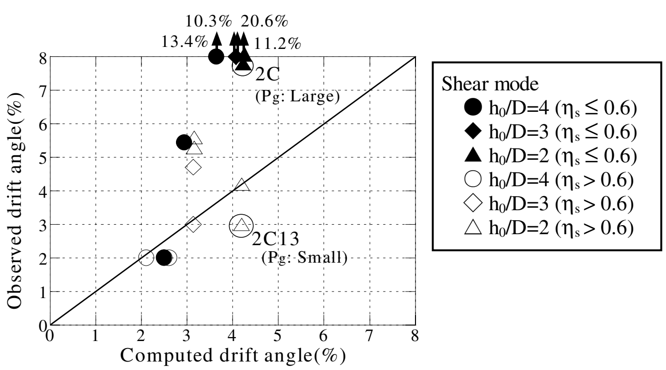

Figure 14: Comparison of collapse drift angle

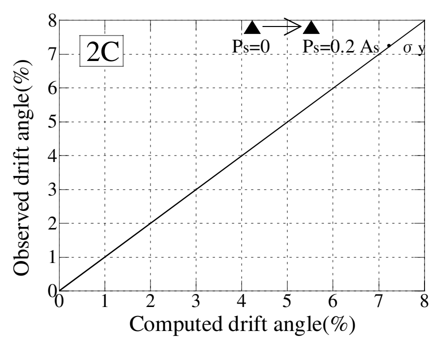

Figure 15: Change of computed collapse drift angle

RELATIONS BETWEEN STRENGTH RATIO AND COLLAPSE IS DRIFT ANGLE

As an index to assess column deformability, a ratio of computed shear strength to computed flexural strength, strength ratio, is often used. The relations between strength ratio and collapse IS drift angle were studied for all specimens including three that yielded in flexure, are shown in Figure 16. The two strengths were computed using conventional equations in Japan.

For the specimens with the shear mode, the results were against the expectation that as the strength ratio increased, the collapse IS drift angle increased. It was mainly because some specimens with large strength ratios showed small values (less than 3%). Most of them were the specimens the bar stress ratios of which were large (η_s>0.6), in other words, p_g was small and/or axial load was large. This implies that the effect of p_g and axial load on the collapse, though included in the strength ratio, is for the above cases more than the extent considered in this ratio. On the other hand, the specimens with the flexure-shear mode met the expectation.

It is interesting to note that there is a big gap in the IS collapse drift angles of No.1 that is largest in the strength ratio among the shear specimens and No. 7 that is smallest among the flexure-shear specimens. And the latter value is about one sixth of the former one. Not only this result is opposed to the general recognition that as the strength ratio increases, deformability increases, but also the difference is extremely large. The problem lies in No.7 that is rather high (0.82) in the strength ratio but very low in the collapse IS drift angle. It is urgent to study the border region of failure modes where the strength ratio is around 0.75 to 0.80.

The relations between strength ratio and IS drift angle at shear failure (flexure failure only for No.8) are shown in Figure 17. The translation of drift angle into IS drift angle was done by the way shown previously. For all specimens, as the strength ratio increased, the IS drift angle at shear failure tended to increase. This suggests the strength ratio may be a good index to express the IS drift angle at shear failure.

It is likely that for the specimens with the shear mode a clear trend was not observed between strength ratio and IS collapse drift angle because the shear failure and collapse did not occur at the same time, while for the specimens with the flexure-shear mode a clear trend was observed between the two because they occurred at the same time.

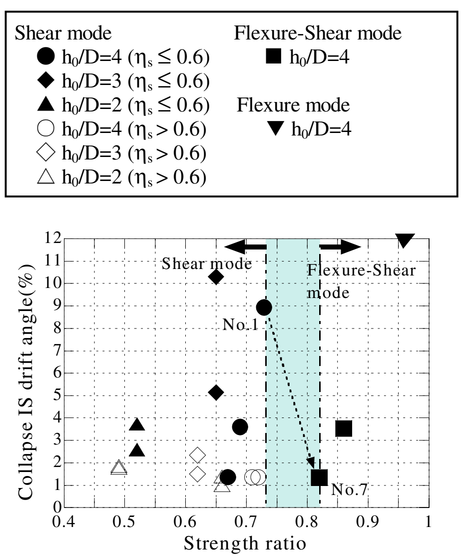

Figure 16: Strength ratio vs. collapse IS drift angle

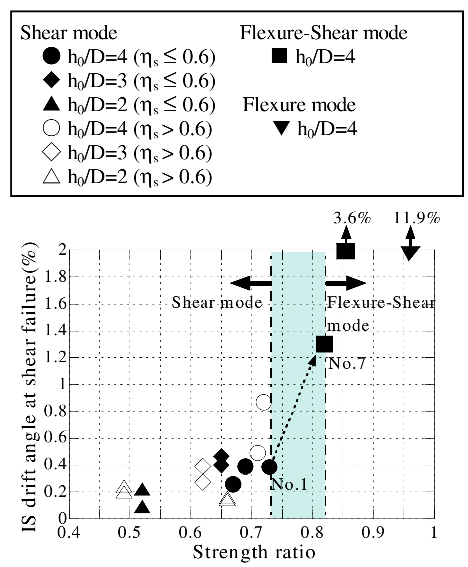

Figure 17: Strength ratio vs. IS drift angle at shear failure

CONCLUSIONS

The major findings from this test and the past tests intended to study the axial collapse of old RC columns are as follows. The range of test variables are as follows: h_0/D=2 to 4, p_g=0.94% to 2.65%, η =0.18 to 0.35 and p_w=0.11% to 0.21%.

(1) Procedures to collapse

The specimens with the shear mode fail in shear when a shear crack occurs at the column middle portion. However, the collapse does not occur at that time. During the subsequent loading, when the shear crack widens and shear force decreases nearly to zero, the collapse occurs. The collapse of these specimens is considered to relate with the increase of axial load carried by the longitudinal bars and the decrease of compression strength of them. On the other hand, for the specimens with the flexure-shear mode the shear failure and collapse occur at the same time at the hinge region, suddenly without any symptom of collapse. The collapse of these specimens is considered to relate with the crushing of concrete.

(2) Relations between η_s and collapse IS drift angle for specimens with shear mode

For the specimens with the shear mode, there is a correlation between bar stress ratio η_s and collapse IS drift angle, indicating this drift angle may be assessed using η_s that includes the effect of p_g and axial load. And if p_w is more than 0.1% and η_s is less than 0.6, the collapse IS drift angle of 1% is secured.

(3) Relations between strength ratio and collapse IS drift angle

For the specimens with the shear mode, the results are against the expectation that as the strength ratio increases, the collapse drift increases, while the specimens with the flexure-shear mode meets this expectation. Such result is believed to be due to the difference in the collapse mechanism of them. It is interesting to note that there is a big gap in the collapse IS drift angles of the specimen that is largest in the strength ratio among the shear specimens and the specimen that is smallest among the flexure-shear specimens. The latter value is about one sixth of the former one. Not only the result is opposed to the general recognition that as the strength ratio increases, deformability increases, but also the difference is extremely large. It is urgent to study the border region of failure modes where the strength ratio is around 0.75 to 0.80.

(4) Equation based on shear-friction model to predict collapse drift angle

For the specimens with the shear mode, the equation based on shear-friction model gives good approximation in case of large values of η_s (η_s>0.6). However, it tends to underestimate the observed collapse drift in case of small values of η_s ($\eta_s \leq 0.6$). It may be because the equation ignores the effect of longitudinal bars on the axial compression carrying capacity, suggesting the possibility of improving the equation if this effect is appropriately included.

REFERENCES

1. Moehle, J. P., Elwood, K. J., and Sezen, H. "Gravity Load Collapse of Building Frames during Earthquakes." ACI SP-197. Behavior and Design of Concrete Structures for Seismic Performance. American Concrete Institute, 2002: 215-238.
2. Nakamura, T. and Yoshimura, M. "Axial Collapse of R/C Short Columns." Proceedings of the fib Symposium - Concrete Structures in Seismic Regions -, 2003: 228-229.
3. Nakamura, T. and Yoshimura, M. "Gravity Load Collapse of Reinforced Concrete Columns with Brittle Failure Modes." Journal of Asian Architecture and Building Engineering, Architectural Institute of Japan, 2002; 1(1): 21-27.